The 18.6-year lunar nodal cycle may affect ecosystems on the Northwest Atlantic continental shelves

Pierre Poitevin, Pascal Lazure, Virginie Roy, Sébastien Donnet, Laurent Chauvaud

Journal of Marine Systems
November 2022, Volume 235 Pages 103783 (14p.)
https://doi.org/10.1016/j.jmarsys.2022.103783
https://archimer.ifremer.fr/doc/00788/89963/

The 18.6-year lunar nodal cycle may affect ecosystems on the Northwest Atlantic continental shelves

Poitevin Pierre [1, 2, *], Lazure Pascal [3, *], Roy Virginie [2], Donnet Sébastien [4], Chauvaud Laurent [1]

[1] Université de Bretagne Occidentale, Laboratoire des Sciences de l'Environnement Marin (UMR6539 UBO/CNRS/IRD/Ifremer), 29280 Plouzané, France
[2] Fisheries and Oceans Canada, Maurice Lamontagne Institute, Mont-Joli, QC, Canada
[3] IFREMER, Laboratoire d'Océanographie Physique et Spatiale (UMR6523 CNRS/IFREMER/IRD/UBO), 29280 Plouzané, France
[4] Fisheries and Oceans Canada, Northwest Atlantic Fisheries Centre, Saint-John's, NL, Canada

* Corresponding authors : Pierre Poitevin, email address : poitevin.pierre@gmail.com ; Pascal Lazure, email address : pascal.lazure@ifremer.fr

Abstract :

As one of the foremost global forcings, tidal circulation exerts a pervasive influence on biological and physical processes occurring in the world's oceans on hourly to decadal time scales. This research identified the 18.6-year periodic variation in the lunar orbital plane within an annually resolved 140-year (1875 to 2015) shell growth master chronology measured from 21 live collected Arctica islandica, a bivalve known to be one of the longest lived non-colonial animals. The potential ecological implications of this result warranted detailed inventory of underlying physical processes. The absence of long-term in situ hydrological data for the bivalve's habitat was circumvented by the use of satellite data and numerical modeling which show that coastal regions of the Northwest Atlantic shelf clearly record diurnal tidal currents influenced by the 18.6-year nodal lunar cycle. The approach described here demonstrates that combining physical and biological data can help to identify subtle ecological processes over long time-scales for accurately disentangling the latter from variation introduced by anthropogenic climate change.

Highlights

► The astronomical 18.6-year nodal tidal cycle (18NTC) influences a bivalve (*A. islandica*) growth variability in Saint-Pierre and Miquelon archipelago (SPM). ► Sea Surface Temperature bidecadal variability in SPM region is partly related to 18NTC. ► 18NTC influences vertical mixing of some regions of the NW Atlantic shelf.

Keywords : Arctica islandica, Tides, Northwestern Atlantic continental shelf, Sclerochronology, Growth

1. Introduction

Marine ecosystems experience environmental forcings over temporal scales ranging from a few hours to several decades. A detailed understanding of these environmental variations and their influence on living organisms on multidecadal time scales is critical for understanding and predicting how ecosystems will respond to anthropogenic climate change.

The marine environment includes parameters that determine benthic invertebrate lifestyles and growth trajectories. Parameters such as temperature, nutrient availability and associated primary production mainly depend on complex ocean-atmosphere interactions, but also on tides, a highly predictable astronomical forcing that particularly influences coastal regions on a synchronized global scale. As deterministic processes, tides appear primarily as semi-diurnal and diurnal variations in sea level, but also exhibit several long-term oscillations including the 18.61-year nodal tidal cycle

(hereafter 18NTC). This cycle arises from the fluctuation of the lunar orbital plane, which on average has a 23.4° angle relative to Earth's equatorial surface, but also varies consistently between 18.3° and 28.6° over a period of 18.61 years. This results in semi-diurnal and diurnal modulation of sea levels and currents that vary according to the lunar and solar components of the tide. The major diurnal tidal components, O1 and K1, have respective periods of 25.82 and 23.93 hours that vary between +/- 19% and 14% (respectively) over a period of 18.61 years. The main semi-diurnal tidal component M2 varies by +/- 4% in phase opposition with the diurnal tidal components (Godin, 1972). For a rigorous description of the nodal cycle see Ray (2007), specifically the comprehensive appendix herein. The 18NTC modulation of sea levels can reach a maximum of 30 cm across continental shelf environments, a range that will contribute to coastal flooding with the ongoing sea-level rise (Peng et al., 2019). However, outside the coastal strip, sea-level variation of a few tens of centimeters with bidecadal periodicity has not been much studied or detected in pelagic or benthic marine environments (Ray, 2007).

Nevertheless, the 18NTC modulation of tidal currents has the potential to influence vertical mixing of the water column by the same well-documented physical processes that govern the ~14-day spring-neap tidal cycles, but over a nearly bidecadal period. This implies that the diurnal tidal currents were stronger worldwide during 1969, 1988, 2006-2007 and weaker in 1978-1979, 1997 and 2016 for the last decades. The reverse is true for the semi-diurnal tidal currents but to a lesser extent. Tidal currents contribute to seawater mixing either through friction on the seabed or by the generation of internal waves that produce strong vertical shear and enhance vertical mixing. Thus, an increase in vertical mixing may lead to greater downward transport of solar heat and greater upward transport of nutrients to the euphotic layer in summer. This transport can lower the sea surface temperature (SST), but increase temperature along the sea bottom (i.e., in the benthic environment). The influence of the 18NTC may thus appear in regions experiencing pronounced diurnal tidal currents due to the stronger fluctuations. This 18NTC effect was first reported by Loder and Garrett (1978) using coastal seawater temperatures records in British Columbia (southwestern Canada). More generally, the North Pacific is a region where water properties can be influenced by the 18NTC. 18NTC signals have in fact been observed in current and temperature data from the Northeast Pacific region (McKinnell and Crawford, 2007), the Bering Sea (Osafune and Yasuda, 2010) and the Northwest Pacific (Osafune and Yasuda, 2006). Only a very few studies have documented 18NTC effects in the Atlantic Ocean. Recently, (Agosta, 2014) showed that 18NTC effects appear in SST variability around the Malvinas Islands (Southwest Atlantic) in association with ocean-atmosphere interactions whose variability may affect summer precipitation in the southwestern Andes.

To our knowledge, the 18NTC has never been detected from individual living organisms, because such detection would require accurate long-term environmental datasets against which to evaluate the growth record. Long-lived, sessile species that continuously build exoskeletons throughout their lives are ideal candidates for detecting the 18NTC signal. The bivalve *Arctica islandica* is the longest lived, non-colonial animal forming periodic growth patterns (Butler et al., 2013). Like other mollusks, this species constructs a shell with distinct annual growth increments defined by annual growth lines formed during periods of reduced growth shell (Schöne, 2013). With this periodic banding, each increment can be articulated into an annual, long-term record. Moreover, if the date of a specific growth increment is known (for example the date of death), it is then possible to assign precise calendar dates to an entire shell record. Based on synchronous changes in shell growth rates, time series of increment widths for specimens having overlapping lifespans and collected from the same locality can be combined to build composite or master chronologies (Schöne, 2013; for a review). Annual increment widths generally record the organism's physiological interactions with its environment (Butler et al., 2013). Although genetic factors can influence ontogenetic growth trends and other fitness-related traits (David et al., 1995), year-to-year variability in shell growth arises mainly from environmental factors (Marchitto et al., 2000).

The site of bivalve sampling is the Saint-Pierre and Miquelon (SPM) archipelago, two small French islands located in Canadian waters located in southwestern Newfoundland (Fig. 1A). Sea level tidal variability is considered semi-diurnal in the region as the M2 and S2 components (0.60 and 0.17 m respectively) dominate the diurnal O1 and K1 components (0.07 and 0.06 m respectively) in Saint-Pierre harbor. Recent studies have shown new characteristics of SPM coastal waters little studied in the past (Lazure et al., 2018; Poitevin et al., 2019). Lazure et al. (2018) showed the extreme variability of the bottom temperatures (> 11.5 °C at depths of 30–60 m) at a diurnal tidal frequency during the stratified period (i.e., late spring to early fall). Furthermore, previous sampling in shallow coastal waters of the SPM (15 m depth) has shown the sensitivity of *A. islandica* to high-frequency dynamics (Poitevin et al., 2020), but also to regional circulation at the scale of the NW Atlantic (Poitevin et al., 2019).

Following further sampling of *A. islandica* in stratified waters, the first objective of this study was to assess a potential 18NTC footprint in *A. islandica* shells at this site theoretically conducive to producing visible traces of 18NTC through modulations in tidal mixing and thus in growth increments of *A.islandica* shells. The converging evidence for this influence then led us to expand our exploration to a regional scale and hypothesize that 18NTC may act on a larger scale on the NW Atlantic shelf.

This paper is organized as follows. In Section 2, we describe *A. islandica* growth patterns over 141 years. Section 3 is dedicated to a spectral analysis of the master chronology and reconstruction of a time series with an 18.6-year period to compare with the astronomical 18NTC. Strong correlations between these two series led us to assess the environmental conditions underlying these long-term modulations. In Section 4, we describe the tidal dynamics around SPM and present its role on temperature variability near SPM. Satellite SST is then used to explore the SST bidecadal variability in SPM and look for a relationship with the 18NTC. We then extend the local SPM SST-18NTC relationship analysis to regional-scale coastal areas around the NW Atlantic. In Section 5, we use a numerical model to verify that areas experiencing bidecadal SST variability in phase opposition with the 18NTC broadly correspond to continental shelf areas where diurnal currents predominate, strongly suggesting that the 18NTC influences vertical mixing in those areas. Our results indicate that the 18NTC may influence marine ecosystems on regional scales. In Section 6, we discuss the limitations of this study and note further analyses that can help resolve areas of uncertainty.

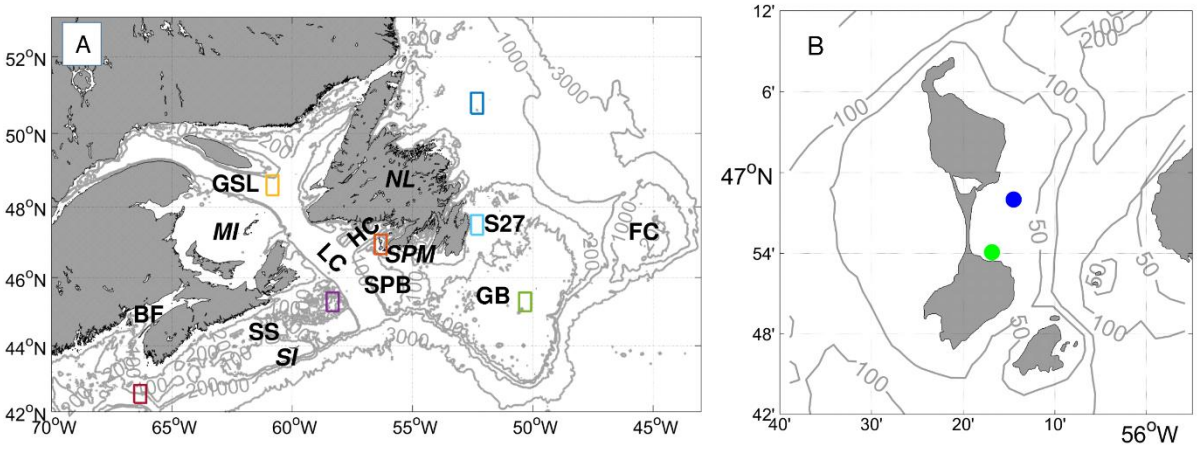

Fig. 1. (A) Location of Saint-Pierre and Miquelon (*SPM*) Archipelago (orange rectangle), *NL*: Newfoundland Island, *MI*: Magdalen Islands, *SI*: Sable Island, GSL: Gulf of Saint Lawrence, FC: Flemish Cap, LC: Laurentian Channel, SS: Scotian Shelf, HC: Hermitage Channel, SPB: Saint-Pierre Bank, GB: Grand Banks, BF: Bay of Fundy. Isobaths (3000, 1000, 200, 100 m) are displayed. Colored rectangles indicate locations of SST time series analyzed in section 4. (B) SPM Archipelago. Blue dot: sampling site (24–25 m depth) for *Arctica islandica* (this study). Green dot: sampling site (14–15 m depth) for *A. islandica* (Poitevin et al., 2019).

2. Construction of *Arctica islandica* master chronology

2.1. *Arctica islandica* sclerochronological preparation

A total of 21 *A. islandica* shells were cut, polished and etched in Mutvei's solution using the sclerochronological procedures described in (Poitevin et al., 2019). Shell sections were then photographed under reflected light (Carl Zeiss, KL 2500 LCD) using an AxioCam MRC 5 installed on a Carl Zeiss SteREO Lumar.V12 stereomicroscope equipped with a motorized stage and adjusted to 25× magnification. Photomosaics were constructed using AxioVision 4.9.1 software (Carl Zeiss) and resulting images were processed with Image J software (NIH Image) to identify and measure the growth increment widths. Increments were measured perpendicular to increment boundaries at a consistent distance, halfway between the outer and inner boundaries of the outer shell layer on the margin (Mette et al., 2016; Poitevin et al., 2019; Schöne, 2013). To obtain a robust annually-resolved chronology, the growth increment series of live-collected specimens were cross-dated since the year of death (2016) of these specimens was known. Cross-dating describes the process of matching temporally overlapping time series based on synchronous growth increment patterns induced by common external drivers. Individual growth increment measurements were initially compiled and statistically analyzed using the dplR program (Bunn, 2008) to aid in intershell year-to-year growth comparisons. The statistical crossdating program COFECHA (Grissino-Mayer, 2001) was also used to further verify the first crossdating results. Errors in the chronology identified by dplR and COFECHA were manually reinvestigated and corrected. This yielded a time series of increment width for each individual (available online: https://doi.org/10.5281/zenodo.6823144).

To develop a master chronology, time series of individual increment widths were detrended using negative exponential functions. This deterministic detrending method was chosen as it largely preserves environmental signals that fluctuate over long time periods (Marali and Schöne, 2015; Peharda et al., 2021; Schöne, 2013).

Growth indices (GIs) were then calculated for each year and each individual by dividing the measured increment width by the predicted increment width (Schöne, 2013) as follows:

$$GI_t = \frac{L_{t+1} - L_t}{L(p)_{t+1} - L(p)_t}$$

Where GI_t is the growth index at time t (in years), $L_{t+1} - L_t$ is the measured shell increment at t and $L(p)_{t+1} - L(p)_t$ is the predicted shell increment length at the same time t.

Individual time series of the GI were then standardized as follows (Schöne, 2013):

$$SGI_t = \frac{GI_t - \mu}{\sigma}$$

where μ is the average of all GI values and σ the standard deviation. The standardized GI (SGI) is a dimensionless measure of how growth deviates from the predicted trend. Positive values represent greater than expected growth, whereas negative values represent less than expected growth.

The quality of the chronology was quantified using the expressed population signal (EPS) statistic (Wigley et al., 1984):

$$EPS = \frac{n * R_{bar}}{\left(n * R_{bar} + (1 - R_{bar})\right)}$$

where R_{bar} is the average of all correlations between pairs of SGI chronologies and n is the number of specimens used to construct the stacked chronology.

Although there is no analytical threshold for this statistic, EPS values higher than 0.85 are interpreted to indicate that the variance of a single SGI chronology sufficiently expresses the common variance of all SGI series. All these analyses were carried out using the R package dplR (Bunn, 2008).

2.2. Growth chronology construction

Twenty-one live *A. islandica* specimens were collected by scuba divers in September 2016 in circalittoral zone (water depths of 24–25 m) along the southeastern shore of the sandy Miquelon-Langlade isthmus (Fig. 1B). The sampling area consisted of homogenous, compacted, stable and well-graded fine-grained sand (85% of its mass between 100 and 200 µm).
The shell-based growth record covers the time period from 1875 to 2015. The shortest and longest individual time series records used to build the master chronology were 32 and 141 years, respectively. The average length of the 21-time series was 78.24 years (1σ = 20.27). Based on the individual growth indices (GI), shells present a strong and synchronous growth pattern among individuals (Fig. 2A). Individual growth records were combined to calculate SGI values (Fig. 2B). These dimensionless measures document how average annual growth deviates from the predicted trend. Positive SGI values represent greater than expected growth, whereas negative SGI values represent less than expected growth. Since the 1980s, even when SGI time series follow a zigzag pattern alternating between high and low values, the SGI values have remained mainly negative, similar to shallower *A. islandica* specimens from SPM (14–15 m depth; (Poitevin et al., 2019)). The running EPS calculated over a 15-year window with 8-year overlap indicates that the variance in individual growth chronology sufficiently expresses the common variance of all GI series after 1905. Synchronous shell growth was also noted prior to this period. The overall series exhibited an intercorrelation of 0.526 and an average mean sensitivity calculated according to Eq. 2 in (Biondi and Qeadan, 2008) of 0.239.

For the sake of comparison, we also interpreted a shell growth master chronology described in (Poitevin et al., 2019) from a nearby *A. Islandica* locality (green circle in Fig. 1B) sampled in infralittoral zone (water depths of 14-15 m) and where the water column is nearly vertically homogeneous. This chronology extends over 166 years (1850-2015) and will be referred to hereafter as the infralittoral SGI.

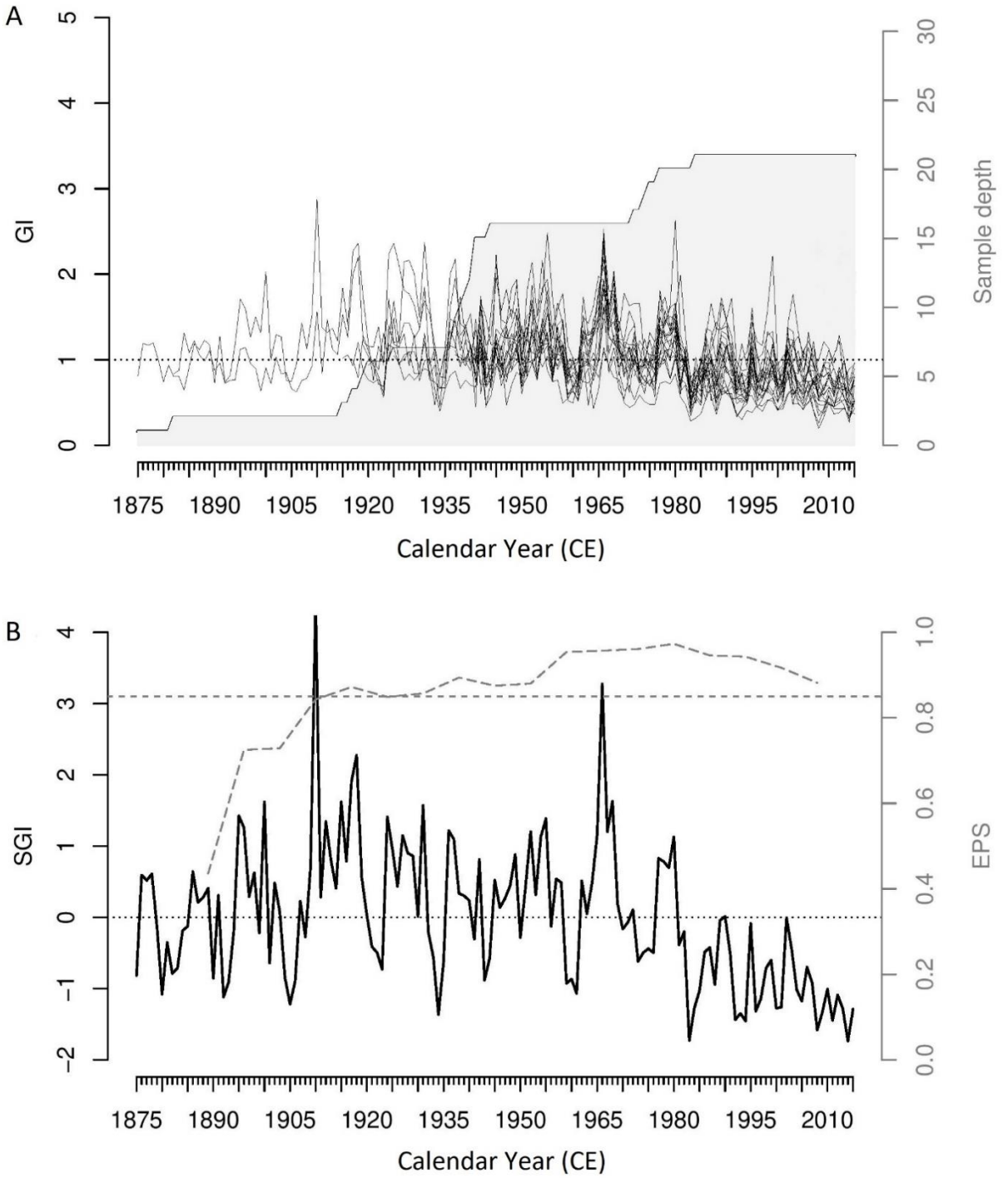

Fig. 2. *Arctica islandica* master chronology. (A) Individual detrended growth index (GI) time series and number of shells used in the chronology (sample depth). The horizontal gray dotted line crossing 1 on the GI axis distinguishes measured annual increments widths larger (GI > 1) and smaller (GI < 1) than predicted (negative exponential functions). (B) Standard growth index (SGI) master chronology (black curve) and expressed population signal (EPS) values (gray dashed curve). The horizontal gray dotted line crossing 0 on the SGI axis distinguishes positive and negative SGI values. The horizontal gray dashed line represents the EPS threshold of 0.85 above which the master chronology is typically considered to be statistically robust (Wigley et al., 1984).

3. Analysis of *Arctica Islandica* master chronology

3.1. Spectral analysis

3.1.1. Methods

Three spectral methods were used to detect frequencies: a Fourier transform, the maximum entropy method (MEM, sometimes called maximum entropy spectral analysis (MESA) (Padmanabhan and Rao, 1988)) and the multi-taper method (MTM) (Thomson, 1982). The fast Fourier transform (FFT) simply considered the entire SGI time series (N=141) for the spectrum shown in Fig. 3A.

The second method (MEM) is an autoregressive model proposed by (Burg, 1967) that allows a better resolution than Fourier transform, but is parametric in the sense that the order of the model must be specified. As model order increases, spurious peaks may appear and results must be interpreted with caution. A wide range of methods can be used to determine model order. This study estimated orders using the panel of frequencies we targeted and assuming a bidecadal period to test for robustness.

The MTM technique (Ghil et al., 2002) uses a set of orthogonal tapers that are designed to reduce spectral leakage. This method can also detect harmonic frequencies and oscillations with constant phase over the entire series. We used the freely available SSA-MTM Toolkit for spectral analysis (http://research.atmos.ucla.edu/tcd//ssa/).

3.1.2 Spectral analysis of the standardized growth index (SGI) and the infralittoral SGI

Figure 3A shows results of the FFT, MEM with different model orders (40 and 50) and the MTM spectral methods for the low frequency (< 1/6.6 year) component of the spectra. The three different methods gave similar results, with three spectral peaks indicating periods of ~18 years, ~13 years and ~10 years for frequencies lower than 0.15 cycles per year (cpy). The infralittoral SGI master chronology (Fig. 3B) shared a common 10-year spectral peak and a 28-year spectral peak detected only by MEM. Interestingly, the ~18 year frequency is not detected in this latter time series. These results led us to continue with the recomposition of the SGI series at periods close to 18 years to compare it with the astronomical nodal cycle.

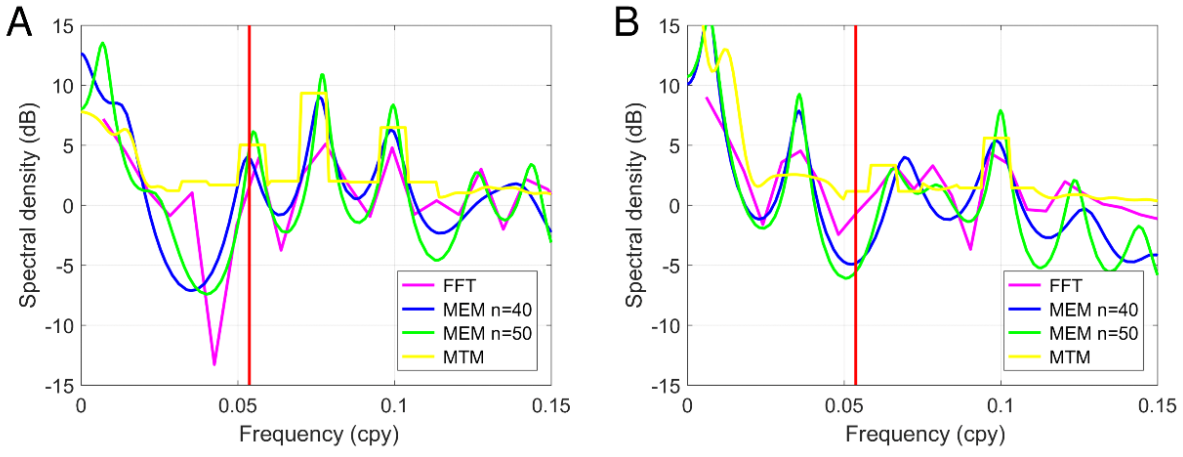

Fig. 3. (A) Power spectra from the standardized growth index (SGI) time series, (B) Power spectra from the infralittoral SGI time series (Poitevin et al., 2019). Fast Fourier Transform (FFT): magenta; Maximum Entropy Method (MEM) with filter length=40: blue, length=50: green; Multi-Taper Method (MTM): yellow. Vertical red line shows the frequency of the nodal tidal cycle (0.0537 cycles per year (cpy) corresponding to a period of 18.6 years).

3.2. Reconstruction of the *Arctica islandica* growth index with an 18.6-year period

3.2.1 Methods

The FFT reconstructions were based on the same series, but truncated of the 11 most recent or oldest years to obtain an integer value for the number of 18.6-year cycles (130/18.6≈7). This truncation allowed to evaluate the spectral density at the frequency of $(18.6\ yr)^{-1}$ and to reconstruct the signal at this specific frequency. The two truncated time series gave similar reconstructions for this period. These were averaged over the shared period and then the entire record was assembled by completing the 11-year beginning and end intervals with each reconstruction. MTM series were reconstructed at the frequency of the detected harmonic line. Two additional methods were used to decompose the SGI time series in sequence of varying frequencies: the empirical mode decomposition (EMD) and the singular spectrum analysis (SSA).

The *A. islandica* SGI and SST time series (see below) were analyzed using EMD (Flandrin et al., 2004; Huang et al., 1998). EMD is a non-parametric and adaptive method that converts time series into a limited number of intrinsic mode functions (IMF) with decreasing frequencies. It does not assume any decomposition basis as trigonometric functions do for the Fourier transformation or as mother wavelets do for wavelet transformation. This method is used in many fields outside of the geosciences, including biomedicine and economics. It uses an iterative approach for which the last series, referred to as the residue, represents the trend of the original series. The main drawback of EMD is the mixing mode, which may cause different IMFs to diverge from an orthogonal orientation, thereby causing overlap of spectral content between neighboring IMFs.

SSA is a non-parametric method (Vautard and Ghil, 1989) that decomposes an original series into a small number of statistically independent components. It uses singular value decomposition of the correlation matrix estimated after embedding the signal into its delayed coordinates. SSA calculates a covariance matrix using the Toeplitz approach and then determines eigenvalues and eigenvectors. The principal components (PCs) are given as scalar products of the eigenvectors and time-delayed embedding belonging to the original series. Reconstructed components (RCs) are calculated by inverting the PCs and calculating the averaged anti-diagonals. The method completely reconstructs original time series by summing all of the reconstructed components. Pairs of equal or nearly equal SSA eigenvalues in approximate phase quadrature (Ghil et al., 2002) define oscillatory modes. We used an adapted version of MATLAB 2016 with the signal processing toolbox program (https://fr.mathworks.com/matlabcentral/fileexchange/58967-singular-spectrum-analysis-beginners-guide) to perform the analysis. The embedding dimension was set to 50 and the reconstruction was done with RCs 5 and 6.

3.2.2 Reconstruction with an 18.6-year period

We extracted the 18.6-year period from the FFT and MTM SGI time series to compare it with a known, idealized 18NTC time series (Fig. 4). We used the formula provided in the appendix (Ray, 2007) to calculate the 18NTC signal with an arbitrarily defined amplitude (+1 to -1).The EMD methods generated six IMFs. The third IMF highlights several nearly bidecadal cycles with eight maxima over 141 years. SSA generated several RCs from which the sum of a pair of RC 5 and RC 6 revealed an oscillation approaching a period of 18 years.

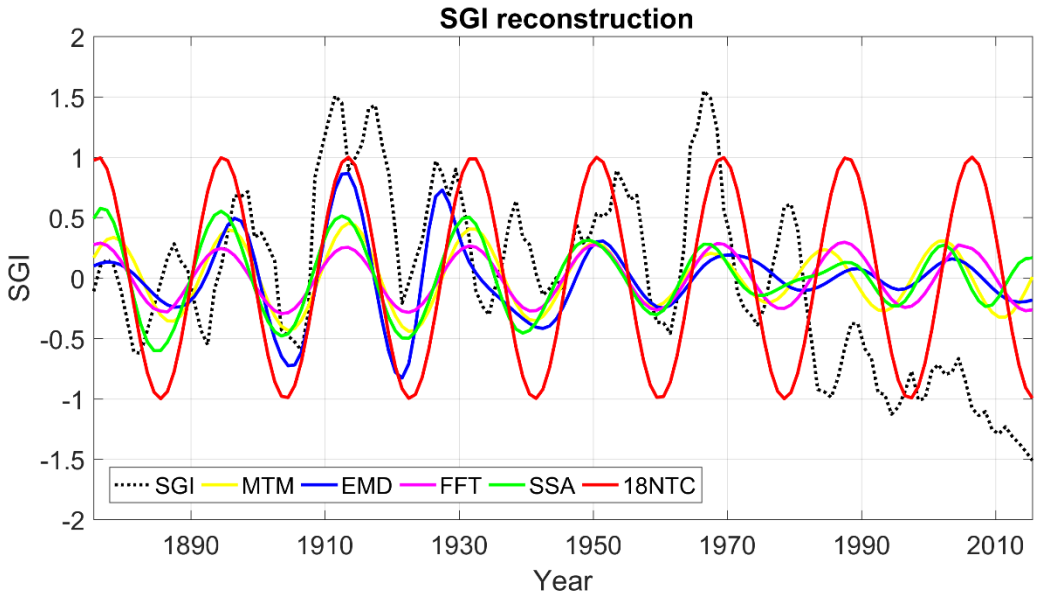

Fig. 4. Master chronology time series reconstructions at an 18.6-year period over time. Yellow line: Multi-taper method (MTM) reconstruction from harmonic components significant at the 95% confidence interval. Blue line: third intrinsic mode function (IMF) from an empirical decomposition method (EMD) analysis. Magenta line: inverse fast Fourier transform (FFT) reconstruction of the 18.6-year period. Green line: singular spectrum analysis (SSA) (M = 45) reconstruction from the sum of reconstructed components (RCs) 5 and 6. Red line: astronomical 18.6-year nodal tidal cycle (18NTC) (arbitrary amplitude). Black dotted line: standardized growth index (SGI) 5-year running average.

All methods (Fig. 4) gave roughly similar results and show that the phases remained constant and consistent with the 18NTC phase until at least the ~1980s/90s. The shell growth anomalies are all in phase with the 18NTC for the eight periods covered by the 1875-2015 timeframe of the SGI. Before the 1990s, phase shifts between reconstructions and 18NTC generally did not exceed two years. Correlation estimates between the reconstructed periodicities and the 18NTC signal varied from 0.66 for EMD to 0.99 for FFT ($p < 0.001$; N = 141) and variance ratios between the reconstructed signals and the SGI (= 1) ranged from 3.8 to 9.7%. These variance ratios increased to 7.3-18.3% when compared with the 5-year smoothed SGI series.

4. Physical background and temperature observations and analysis

4.1. Tidal dynamics and hydrology in the Saint-Pierre and Miquelon archipelago

A recent study (Lazure et al., 2018) based on observations of coastal water temperature at 30 and 60 m depth around SPM detected strong diurnal tidal currents and diurnal bottom water temperature oscillations exceeding 10°C during times of maximum summer stratification. These observations were interpreted as an expression of a coastal trapped wave resonant with the diurnal frequency of the tide rotating clockwise around the archipelago within two periods. On the eastern side of the archipelago, the main semi-diurnal component M2 was of the same order of magnitude as the diurnal components, but it was much weaker on the western side. In this study, only the temporal evolution of the bottom temperatures was measured and we lacked observations in the water column except the currents measured by Acoustic Doppler Current Profiler (ADCP). This absence of measurement was supplemented with a SPM2017 oceanographic cruise, which consisted in measuring the temperature profiles around the archipelago for one month.

4.2. Hydrology

4.2.1. Seawater temperature measurements around Saint-Pierre and Miquelon

Moored thermistor chains with various numbers of probes were deployed during the SPM2017 cruise from 13/08/2017 to 10/09/2017. At each mooring, two temperatures probes were set at the surface and the bottom and the rest of the probes were evenly distributed along the line (total of 3, 5 and 9 probes at 15, 30, 80 m depth, respectively). Each probe measured temperature and pressure and was packed in a small plastic bag filled with Marcol 82 insulating oil. The acquisition time step was 2 minutes. Vertical temperature profiles result from linear interpolation every 2 m from the bottom between two probes by taking into account the vertical location of each probe measured by the pressure sensor.

4.2.2. Variation in temperature vertical profiles over time

The SPM 2017 cruise extended the dataset of observations at three locations (Fig. 5). Stratification varied from nearly homogenous in shallow waters (Fig. 5C) to a maximum of 16.5°C difference between surface and bottom temperatures (Fig. 5A). In shallow waters, vertical mixing was almost permanent (Fig. 5C). Note that this site is very close to the infralittoral SGI sampling site, but the years of observation differ. Temperatures were measured near the *A. islandica* sampling site (Fig. 3B) in Summer 2017 and show strong stratification and enhanced temperature variability near the bottom, confirming previous observations (Lazure et al., 2018). A diurnal signal clearly appeared with the superposition of a 2-day period, probably related to the wind effect as described in (Bezaud et al., 2020). The last station (Fig. 3A) is located on the north side of St. Pierre Bank and is the first known measurement of the temporal evolution of the temperature profile at the confluence of the Laurentian and Hermitage channels. The measurements show a clear diurnal signal, which consists of an internal wave of ~20-60 m range once a day. A tidal harmonic analysis (not shown) indicates that the main period corresponds to the O1 (25.8 h period) tidal component.

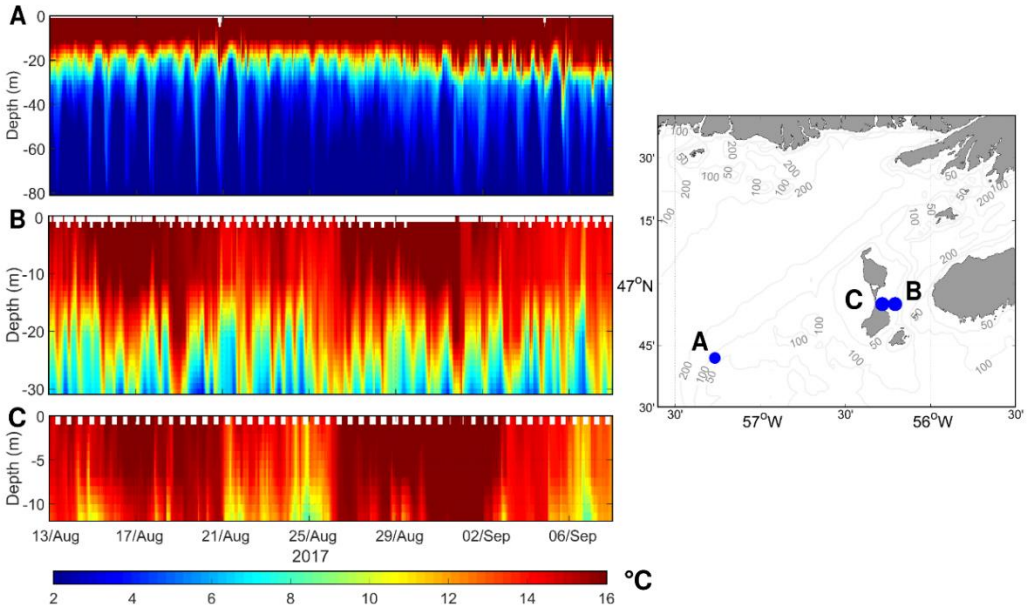

Fig. 5. *In situ* measurements of seawater temperature in °C (color scale displayed in the figure's bottom) over time and depth at 3 mooring sites near the Saint-Pierre and Miquelon archipelago (graphs A, B, C) from 2017/08/13 to 2017/09/08. The corresponding mooring locations (A, B, C) are represented by blue dots on the right panel. Blue dot (A) is located at the northern edge of the Saint-Pierre Bank (80 m depth) while (B) and (C) are situated to the east of Miquelon Island (30 m and 15 m depth).

These measurements confirm the dominant nature of the diurnal tides in SPM area extended to Saint-Pierre Bank. However, on longer time scales, we lack observations taken on a regular basis during the 20th century to evaluate the potential presence of a nearly bidecadal cycle in environmental parameters. The only available multidecadal observations for SPM waters were SST satellite data extending back to September 1981.

4.3 Analysis of SST in Saint-Pierre and Miquelon and the Northwest Atlantic

4.3.1. SST data set

Long-term temperature analysis used the Pathfinder V5.3 dataset (Saha et al., 2018) with a squared grid cell resolution of about 4 km. Data were rendered homogeneous with respect to the different satellites, which allowed data aggregation on a daily basis with the quality levels provided. Given the volume of missing or low-quality data for the study area, we aggregated data into rectangular grid boxes spanning 33' in latitude and 30' in longitude (i.e., 61x38 km), an area roughly the size of the SPM archipelago and its coastal waters. SST data with quality indices between 5 and 7 (the maximum quality) were extracted and spatially averaged. Given the significant cloud cover in this region, the month offering the minimal amount of missing data was August and the ratio of clear pixels to total available did not exceed 0.20 (Fig. A1). All analyses were thus performed using August-averaged SSTs over the 37-year time series (August 1982-August 2018). The reliability of the dataset was tested by comparing it with the only long-term *in situ* measurement series available (Station 27, e.g., Drinkwater et al., 2013). The results were found to be sufficiently convincing (Fig. A2) for further analysis of this spatially aggregated dataset.

4.3.2. Extraction of the nodal cycle in the sea surface temperature time series at Saint-Pierre and Miquelon

An SST time series from the grid box including SPM (location on Fig. 1) was extracted and analyzed using EMD methods and a simple least square method (LSM) to highlight a potential nearly bidecadal cycle from SST. This analysis was challenging due to the limited length of the time series, which could only represent two cycles at best. Unlike LSM, which consists in fitting a sine function of 18.6-year period on the time series, EMD does not make any a priori assumption on the periods of the different IMFs. The results of the two methods (Fig. 6) show similar amplitudes (~1°C) and variances of ~10% relative to total SST variance. A slight and varying phase shift occurs between the two methods, but does not exceed 2 years. Pearson's correlation coefficients calculated for the 18NTC and SST series at 18.6-year period were significant ($p < 0.002$; N = 37) and ranged from -0.94 for LSM to -0.54 for EMD. Negative correlations indicate that years with high 18NTC (i.e., stronger diurnal tidal currents) correspond to greater vertical mixing and therefore lower SST around SPM during August when thermal stratification of the water column is most pronounced.

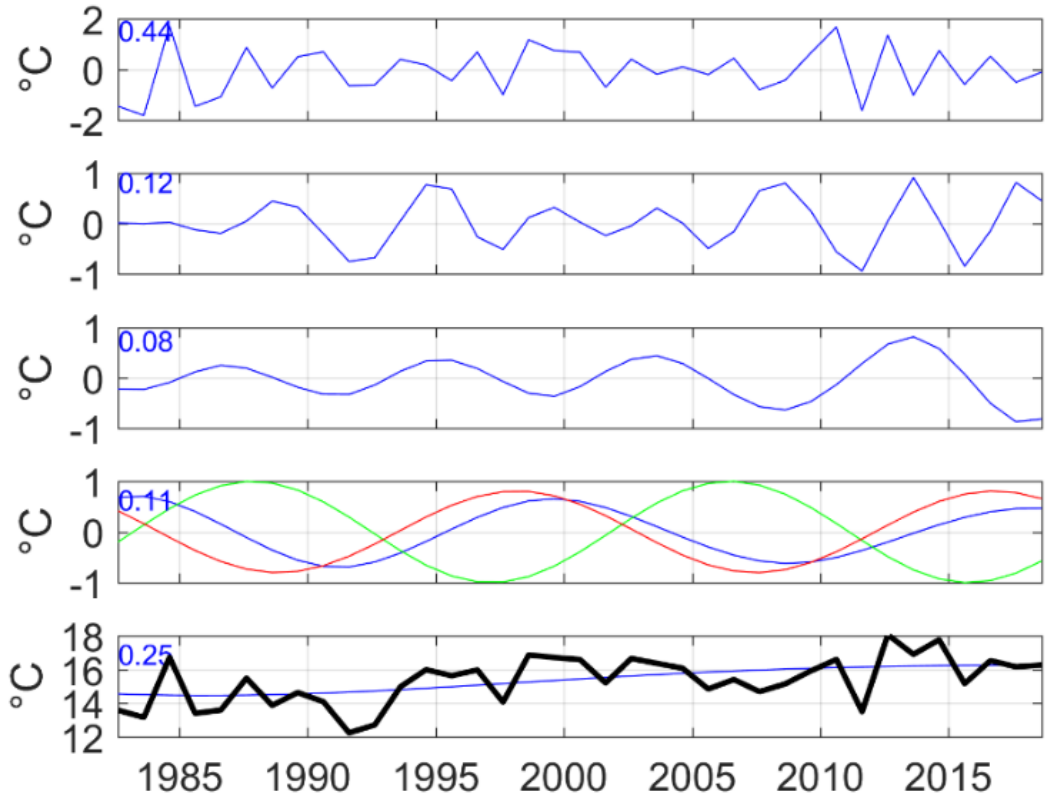

Fig. 6. Intrinsic mode function (IMF) time series from empirical decomposition (EMD) (blue lines) of August satellite sea surface temperature (SST) data from Saint-Pierre and Miquelon (orange rectangle in Fig. 1) over time. Bottom panel: SST time series (heavy black line) and residue (in blue). Panel IMF4 (second from bottom panel): 18.6-year nodal tidal cycle (18NTC) (green line), least square means (LSM) reconstruction minus the time average (red line) and fourth IMF (blue line). The number in the upper left corner indicates the ratio of the IMF variance to the sum of each IMF variances.

4.3.3 Extension to the Scotian-Newfoundland shelves

Taking advantage of the availability of a spatialized SST dataset and the apparent influence of the 18NTC around SPM, we extended our exploratory SST analysis to the regional level with LSM. Selective tests were carried out on the phase value of the fitted SST time series by comparing the phase of the LSM series with the 18NTC phase (i.e., 67° GMT). We tested whether the LSM with phase opposition to the 18NTC within a range of +/- 1 year (corresponding to +/-19°, i.e., 360°/18.6 yr) may be due to the 18NTC influence. Outside this range, LSM results are considered to result from causes other than tidal mixing. As an example, several time series of August SST and the result of their LSM compared with the 18NTC are shown in Figure 7. As expected, higher temperatures were found south of the Scotian shelf, whereas lowest temperatures were found north of Newfoundland. By fitting an 18.6-year period sine to these time series, the upper range of temperature variabilities (~1°C) satisfied the phase test criterion.

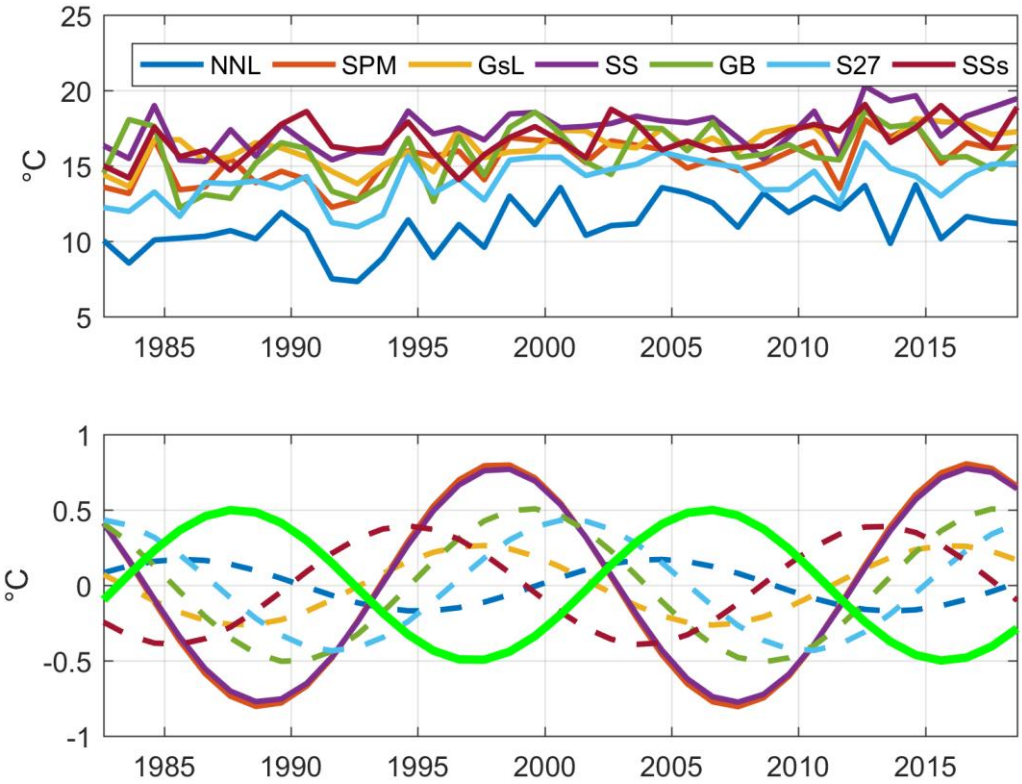

392

393 **Fig. 7**. Upper panel: August satellite sea surface temperature (SST) time series extracted from the
394 corresponding color boxes displayed in Fig. 1. Acronyms are defined in Fig. 1 except NNL (North
395 Newfoundland) and SSs (South Scotian shelf). Lower panel, green curve corresponds to the 18.6-year
396 nodal tidal cycle (18NTC) (arbitrary amplitude of 0.5). Other curves correspond to the result of the
397 August SST least squares mean (LSM) minus the mean of each series. Dotted lines represent time series
398 which do not satisfy the phase test criterion (see text), whereas continuous lines (SPM and SS) do.

399 LSM was applied to the whole area and SST variance of grid boxes whose phase was not
400 between -132° and -94° (18NTC phase +- 1 year) was set to zero. Figure 8 displays the ratio of the
401 variance of the boxes satisfying the phase criterion to the variance of the SST time series. This analysis
402 highlights areas located near SPM to the west such as Saint-Pierre Bank, south of Magdalen Islands,
403 and eastern and offshore parts of the Scotian Shelf and the entrance to the Bay of Fundy.

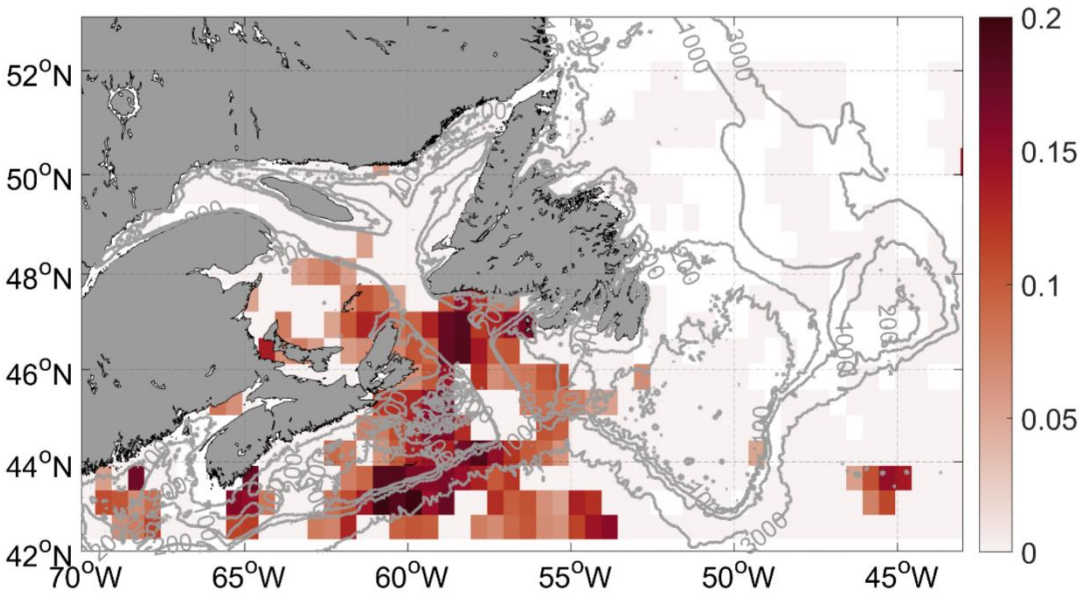

Fig. 8. Ratio of satellite SST variance (color scale on the right) for Least Square Method fitted SST series extracted from each 33' latitude and 30' longitude boxes whose phases are in opposition to the 18.6-year nodal tidal cycle (18NTC series) by +/- 1 year. Gray lines represent 3000, 1000, 200 and 100 m isobaths.

In the vicinity of the outer Laurentian Channel, part of the long-term variability of the SST is in phase opposition with the nodal cycle. To verify that tidal mixing may be the explanatory factor, we used a numerical model to verify the nature and magnitude of tidal currents and their contribution to vertical mixing.

5 Numerical modeling of tidal currents

5.1 The model

The MARS2D model was used to calculate barotropic tidal currents over the study area. The model used a 2 km square grid size and was forced along open boundaries by tides extracted from the FES 2004 database (Lyard et al., 2006). Simulations ran from 2014/01/01 to 2014/03/16 with a spin-up of 0.5 months and have been shown to accurately reproduce tidal sea levels and currents (Bezaud et al., 2020). The barotropic tidal currents were passband filtered (5^{th} order Butterworth filter) to extract semi-diurnal (3-15 h) and diurnal components (18-30 h).

5.2 Tidal mixing with emphasis on the diurnal tidal current contribution

As first demonstrated by (Simpson and Hunter, 1974), tidal mixing by barotropic currents depends on the action of frictional forces on the bottom, which can be quantified by the ratio of water depth to the cube of velocity, an estimate known as the Simpson-Hunter parameter. The lower the value of this parameter, the greater the vertical mixing. As shown by (Garrett et al., 1978), the transition from well mixed to stratified conditions occurs when $H/U^3 = 70\ m^{-2}.s^{-3}$ (4.2 in log scale) with H the total depth (m), U the tidal current ($m.s^{-1}$). We calculated the time-averaged value of the Simpson-Hunter parameter from hourly simulation results over the duration of a month for both diurnal and semi-diurnal currents. Figure 9 shows Simpson-Hunter parameters (log scale) for diurnal currents where these do not exceed semi-diurnal ones. The calculation highlights areas where diurnal currents predominantly generate vertical mixing, i.e. those likely to experience the most pronounced 18NTC modulation. These areas include SPM, north of the Saint-Pierre Bank, the southeastern edge of

the Magdalen Islands and some locations along the Scotian Shelf off Sidney Bight and along the offshore edge of the Scotian Shelf near Sable Island.

These areas share a number of spatial similarities with those showing a phase opposition between the bidecadal variability in SSTs and the 18NTC (Fig. 8). These similarities suggest that the lunar nodal cycle influences SST and tidally driven vertical mixing in these areas. Along the continental shelf, vertical mixing affects not only temperatures, but also nutrient concentrations and primary production at the surface and throughout the water column. Although measurements below the surface and from near-bottom areas are not available over the duration necessary to validate this assertion, we hypothesize that increased vertical mixing (during 18NTC+) would decrease SST, increase bottom temperatures and thus promote the growth of *A. islandica*. These effects could provide an explanation for the strong positive correlation between low-frequency variability in growth and the 18NTC (Fig. 4).

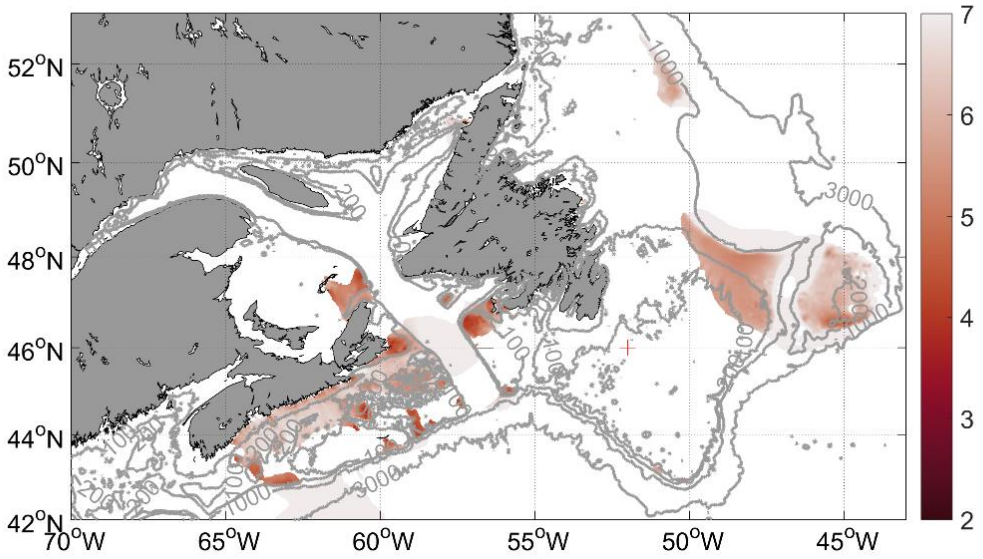

Fig. 9. Simpson-Hunter parameter (colored logarithmic scale displayed on the right) calculated over a duration of a month from diurnal currents obtained from Bezaud et al. (2020) model simulations ran from 2014/01/01 to 2014/03/16 with a spin-up of 0.5 months and shaded when its value is lower than the Simpson-Hunter parameter calculated for semi-diurnal currents obtained from the same model simulations. Gray lines represent 3000, 1000, 200 and 100 m isobaths.

6 Discussion

The results interpreted here derive from three different and independent datasets. These include a combined 141-year growth record from a bivalve species living in SPM coastal waters, monthly SST measurements over a 37-year period and simulations of barotropic tidal currents on a monthly time scale. The two sets of observational data allowed us to identify positive correlations between the 18NTC and *A. islandica* growth chronology (Fig. 4) and negative correlations between the 18NTC and SST (Fig. 8). The schematic modeling step helped reveal a link between SST and diurnal mixing. The remarkable spatial concordance in areas showing a phase opposition between SST and 18NTC and those where strong tidal diurnal mixing prevails (Fig. 9) offers strong arguments to infer the physical process involved.

Hydrodynamic and ecosystem variability in the NW Atlantic has been studied intensively for decades, but to our knowledge this is the first time that the influence of 18NTC has been explored (with the exception of sea level, for which the nodal cycle has long been known). Below, we discuss the limitations of our results. Our arguments in support of a significant influence of 18NTC on local and regional hydrodynamics and ecosystems can be addressed in four questions: How reliable is the detection of 18NTC in bivalve shells? How does mixing impact shell growth? Is our SST analysis relevant for estimating bottom temperature variability and can other factors explain the bidecadal variability? Is this mixing really a result of the diurnal component of the tide?

6.1 Evaluation of the reliability of the nodal tidal footprint in the growth of *Arctica islandica*

The question of whether individual organisms respond uniformly to common environmental influences can be addressed by evaluating the consistency of growth signals within a population (e.g., Douglas, 1920; Mette et al., 2016). The expressed population signal (EPS) established from contemporaneous specimens of *A. islandica* collected around SPM (ca. 25 m depth, in a ca. 400 m^2 area), showed highly synchronized growth patterns. In our study, EPS values exceeded 0.85, the assumed analytical threshold (Wigley et al., 1984), from 1905 to 2015 (Fig. 1D). The series inter-correlation (0.526) and mean sensitivity (0.239) were comparable to those interpreted from other bivalve, fish and tree records (e.g., Black et al., 2005; Helama et al., 2007; Poitevin et al., 2019). Growth patterns in the different shells analyzed showed good agreement. The detrending method used to remove ontological trends may however have influenced the detection of low frequency spectra from the SGI master series. We tried to limit this uncertainty by analyzing individuals of different ontological age and by using a deterministic detrending method that preserves long-term environmental signals (Marali and Schöne, 2015; Peharda et al., 2021; Schöne, 2013). Details of the general approach to detrending and potential associated biases are fully described in previous studies (Butler et al., 2010; Schöne, 2013). Thus, the inclusion of shorter series in the chronology and the preservation of medium- and low-frequency variability by any detrending method (including negative exponential) is limited in practice to wavelengths of about one-third of the average length of the time series (Butler et al., 2010). In our case this allows us to confidently investigate wavelengths shorter than ca. 25 years (as the 18NTC). The present study also highlights that removal of age trends from *A. islandica* (and other bivalves) increment width chronologies remains a major challenge to fully exploit their growth records as no detrending technique is currently specifically developed for bivalve sclerochronologies (Schöne, 2013). The population sampled for this study was dense (> 10 individuals.m^{-2}), living buried in sediment (> 1 cm bellow the sediment surface), not heavily preyed on and not harvested or otherwise disturbed by human activity. Thus, our master chronology was interpreted to offer consistent coverage of *A. islandica* growth conditions in the study area.

The spectral methods used in this study gave similar results and each detected a subtle, but significant spectral peak with a period of about 18.6 years (Fig. 3A). Extractions of the 18.6-year period from the master series using different methods showed that *A. islandica* experiences increased growth during 18NTC maxima and reduced growth during 18NTC minima (Fig. 4). However, importantly, the influence of 18NTC on *A. islandica* growth appears to have decreased since the 1990s. This decline in the influence of 18NTC can be attributed to a decrease in increment size during the last years of life of the studied animals or to the enhanced influence of other environmental forcings exacerbated by global climate change over the past 30 years. Nevertheless, evidence of an 18NTC signal in *A. islandica* shells raises the question of the ecological mechanisms involved in the link between growth and the 18NTC signal.

6.2 Impact of tidal mixing on *A. islandica* growth

Studies have shown that *A. islandica* growth depends primarily and by varying degrees on temperature and food quantity, quality and availability (Ballesta-Artero et al., 2017; Butler et al., 2010; Marali and Schöne, 2015; Mette et al., 2016). Schöne (2013), in his review, suggested that *A. islandica*

through endogenous rhythms can anticipate environmental changes such as ebb or neap tides and associated changes in food availability and temperature. At the ecosystem level, Witbaard et al. (2001) demonstrated the effect of tidal resuspension on benthic food quality by studying growth of three macro-benthic organisms (including *A. islandica*) from two sites from the Southern North Sea. Recent studies of infralittoral water (15 m depth) *A. islandica* paleoenvironmental records for SPM have shown that growth depends most strongly on coastal water temperature and primary production (Doré et al., 2020; Poitevin et al., 2019). These studies however analyzed shells that developed in a practically homogeneous vertical (Fig. 5C) water column and noteworthily these shells did not experience variability with an 18.6-year period (Fig. 3B). At the circalittoral sampling site in the present study, temperature data from the end of summer showed strong vertical temperature stratification and considerable variation on time scales of a few hours (Fig. 5B). Variation in vertical temperature structure can strongly affect primary production. Although *in situ* measurements on primary production in the water column or near bottom are not available, the general dynamics described above have been observed and likely operate in comparable environments. Tides represent one of the dominant physical processes causing vertical mixing on continental shelves (e.g.Sharples, 2008). A recent study of a mid-latitude area with seasonal stratification and moderate tidal currents similar to those observed around SPM (Zhao et al., 2019) found that tidal forcing replenishes nutrients in the upper part of stratified water columns during the summer and thereby both sustains and increases primary production in the surface layer and within the pycnocline. This study and others like it have revealed consistent patterns of variability between primary production and spring-neap tidal cycles (with periods of ~14 days). Spring tides increase mixing and thus cause an increase in primary production and bivalve food availability during stratified period, as long as the turbidity induced by sediment resuspension does not constrain productivity by limiting light transmission (e.g., McSweeney et al., 2017). These tidally driven ecological mechanisms occurring in summer are very likely to influence *A. islandica* growth as, although we have not conducted specific intra-annual growth studies in SPM (given the limited access to this study site), Schöne et al. (2005) demonstrated that *A. islandica* shell collected from the southern and central North Sea reach maximum daily growth rates in August.

Other mechanisms could also explain the 18NTC effect on *A. islandica* growth. Those lie on sediment water interface circulation and the effect of tidal currents on the sorting of sediment and/or food particles, which could possibly influence their quality and bio-availability for *A. islandica*. These tidally driven mechanisms have previously been suggested by Witbaard et al. (2001) which demonstrated their interacting effects on food quality, resuspension, aggregate formation and sediment type to explain *A. islandica* growth variability in the southern North Sea. However, the absence of such sediment water interface environmental measurements in SPM does not allow us to further investigate these aspects in the present study.

Tidal mixing in regions like SPM where diurnal components dominate tidal currents can influence primary production and primary consumer growth due to the ecosystem's sensitivity to changes in tidal current speeds. Moreover, sediment characteristics limit resuspension around SPM (Robin, 2007). Thus, the subtle changes induced by the 18NTC may contribute to the strong positive correlations observed between reconstructed *A. islandica* growth patterns and the nodal tidal cycle. The observed patterns are also very consistent with the infralittoral SGI analysis, which does not display a spectral peak at the 18NTC period, because the spring-neap tide cycle has only a weak influence on ecosystems in almost vertically homogeneous shallow waters.

6.3. Are other processes at play?

6.3.1 Temperature analysis

In this region of the Atlantic Ocean, the only reliable and continuous coastal data available over several decades (in addition to sea level records at tide gauges) are the satellite SST. We are aware that this parameter is a poor descriptor of the bottom temperatures because it also incorporates

advection due to general circulation and variability of ocean-atmosphere exchanges that can mask the effects of vertical mixing. We chose to use only best quality gridded products. This choice strongly constrained the spatial and the temporal resolution of the analysis because we had to perform spatial averaging and only the month of August proved to be usable. Fortunately, this month corresponds to the month when the stratification is maximal and the effect of 18NTC is potentially the most visible. Note that we did not employ the OISST database (Reynolds et al., 2007), which consists of filling the gap by assimilating *in situ* data. The results of the assimilation process vary according to the available data, which are very variable in time and space. It is therefore difficult to estimate their reliability at fine spatial scales. Analyses with this dataset nevertheless yielded roughly the same results (not shown).

It was tempting to use other datasets that have direct measures of bottom temperature, rather than inferring it from the SST. However, we rejected these datasets for several reasons. Databases such as EN4 (Good et al., 2013) were excluded due to their low spatial resolution and their poor consideration of continental shelves. Another alternative would have been to analyze hindcasts, i.e. model results with assimilation of observations (satellite SST, SSH, *in situ* observations), the main problem is that the models considered do not explicitly treat tides. For example, Simple Ocean Data Assimilation 3 (SODA3) (Carton et al., 2018) parameterizes tidal mixing over shelves, but ignores its diurnal components and the nodal cycle. GLORYS (Lellouche et al., 2018), based on the NEMO model, does not take tides on the continental shelves into account. The ability of the assimilation process to correct this bias depends on the density of observations, which is highly variable in space and time. Moreover, in the case of bottom temperatures, only *in situ* measurements (the rarest) are likely to correct these biases. As an example, GLORYS data in the Mid-Atlantic Bight (south of our study area), although very close to reality in general, show the largest errors over Georges Bank (Chen et al., 2021), an iconic area known for its frontal dynamics related to tidal mixing (semi-diurnal in this case) (e.g., Guida et al., 2013). The hindcast shows (Chen et al., 2021, their Figure S2) surface temperatures that are too warm and, conversely, bottom temperatures that are too cold at monthly and at interannual time scales. These discrepancies clearly indicate an underestimation of mixing that data assimilation — although numerous in this well-studied area — fails to correct. Therefore, our SST analysis is based solely on observations, because using any of the datasets described above would not have led to a robust conclusion whatever the outcome, given their biases.

However, to draw robust conclusions on bottom temperature variability, we must show that other physical processes are unlikely to be involved on bidecadal time scales.

6.3.2 Have bidecadal cycles ever been suspected or observed in the study area?

Considerable scientific literature is devoted to describing circulation and hydrology on the NW Atlantic shelf and slope on seasonal to multidecadal time scales. The hydrology and dynamics of this region are particularly complex given that it is the meeting site of the Labrador Current and the Gulf Stream. For example, (Nigam et al., 2018) showed the importance of decadal variability, which results from low frequency variability of the atmospheric North Atlantic Oscillation (NAO). (Wolfe et al., 2019) reviewed the time scales involved in Gulf Stream fluctuations. They range from 7.5 to 13 years. It appears that the north-south migration of the Gulf Stream has a dominant period of 9 years, which could partly explain the peaks observed with a 10-year period on the growth of *A. islandica* in the spectra of the two series (Fig. 3). This study is very consistent with the results of (Poitevin et al., 2019) that show a strong correlation between *A. islandica* growth and the latitudinal position of the shelf-slope front. Moreover, (Halfar et al., 2011) also found decadal periods in coralline algae growth records along the eastern side of Newfoundland, which reflect the Labrador Current influence.

From the literature on the variability of hydrology in the region, we did not note any observations on a bidecadal scale. Nevertheless, bidecadal sea-level cycles in the entire Atlantic Ocean (North and South) have been detected (Vianna and Menezes, 2013) in the SODA model and these

oscillations may be a fingerprint of the Atlantic meridional overturning circulation (AMOC) sea-level variations, which may affect shelf dynamics. The Vianna and Menezes (2013) study reported a regime shift since the beginning of the 1970s that includes all of our SST time series. If confirmed, an AMOC-influenced cycle precludes attributing the observed bidecadal cycle to tidal dynamics. However, no influence of these cycles on coastal surface temperatures has ever been reported since the Vianna and Menezes (2013) study, and it is unlikely that the phase of these oscillations varies across the regional scale (from the Scotian shelf to Labrador shelf) due to the basin-wide scale considered in this study.

6.4 Diurnal tidal mixing on the Northwest Atlantic shelf

The role of diurnal tidal currents in this region has not been extensively studied, probably because the semi-diurnal tidal range dominates throughout the region (with the exception of the Gulf of St. Lawrence, in which an M2 amphidromic point occurs). These currents can potentially be more important than the ratio of semi-diurnal tidal amplitudes to diurnal components would suggest. The diurnal waves are subinertial (periods (24-26 h) > inertial period≈17 h) and the diurnal waves take on features of a coastal trapped wave that results in local current amplifications generally near steep slopes. Indeed, some strong diurnal tidal currents have been described at the edge of the Scotian and Newfoundland shelves (Ohashi et al., 2009; Xu and Loder, 2004, respectively) and more locally near Sable Island (Greenan et al., 2014) or SPM (Lazure et al., 2018).

A recent study (Wang et al., 2020) investigated the impact of tidal mixing in the NW Atlantic shelf using 3D numerical modeling. This study consisted in simulating circulation and hydrology with realistic forcing by comparing the results with or without taking into account the tides represented by the five major constituents (M2, N2, S2, K1 and O1). As expected, the non-tidal simulations showed higher SSTs and lower surface salinities for the month of August due to lower vertical mixing. Examination of the different terms that are at stake in temperature variability, including horizontal advection, showed that bottom temperatures depend locally on vertical diffusion (their Figure 17l). Interestingly, the areas where this mixing had the most impact broadly coincided with the areas we highlight in Figure 9. Unfortunately, the authors considered the tide as a whole and did not attempt to distinguish the effects of the semi-diurnal and diurnal components. However, the earlier work of (Han and Loder, 2003) had already noted that the diurnal K1 currents in the NW Scotian shelf were amplified by the resonance of the first-mode continental shelf wave. They suggested that vertical mixing in this area is probably mainly influenced by diurnal currents, because the O1 wave (of the same amplitude as K1 in this area) had not been considered in their study.

However, a barotropic model has its own limitations, because it does not take into account stratification and associated baroclinic currents. Barotropic tidal interaction with steep bathymetry in a stratified environment during the summer results in internal waves. Waves having diurnal periods are subinertial and therefore trapped by bathymetry (e.g.,Huthnance, 1978). They propagate alongshore leaving the coast on their right in the northern hemisphere. The temperature measurements shown for Saint-Pierre Bank (Fig 5A) suggest strong internal dynamics, which most likely indicate a coastal trapped wave. This coastal trapped wave strengthens the near-bottom currents, causing significant shear in the cross-shore direction and contributes to increased vertical mixing in the alongshore direction. These limitations could explain why the barotropic model does not show strong mixing in the middle of the outer Laurentian Channel (depth range: 200-400 m), while the SST analysis shows strong bi-decadal variability at 46-47°N latitude.

As a result, the areas that we designate as being under the dominant influence of diurnal mixing are in good agreement with the above-cited papers and their extent is probably underestimated due to the limitations of the barotropic approach. The transfer of time scale from diurnal tide to nodal cycle is based on the stronger theoretical modulation of the diurnal vs. semi-diurnal components (see above). Noteworthily, this modulation is globally verified by observations (Cherniawsky et al., 2010), even though there are small observed deviations from the theory that are not yet fully understood.

6.5 Concluding remarks

Based on the annual growth lines of a large and consistent sample of *A. islandica* shells (21 individuals) at SPM, we highlighted here the footprint of an 18.6-year cycle that accounts for about 10% of the interannual variance in growth. We showed that this oscillation is in phase with the lunar nodal cycle (18NTC). From this observation, which is to our knowledge the first one made based on hard parts of animals, we developed an argument to explain the chain of interactions between tidal potential and bivalve growth on the sea bottom.

Based on previous studies of 18NTC, we hypothesized that diurnal tide-induced mixing is also the process underlying these observations on the NW Atlantic shelf. Examination of the August SSTs over 37 years and the use of a numerical tidal model led us to suggest that beyond the SPM archipelago, the Laurentian Channel environment may be partly affected by 18NTC. We also point out several caveats in our arguments that result mainly from the lack of observations spanning several decades. However, the explanatory elements that we provide seem coherent and convincing.

To confirm (or invalidate) our results, several avenues must be explored:

- Since our oceanographic analysis hinges on relationships with diurnal tide-induced mixing and SST, future sclerochronological work should naturally include the second most commonly used proxy in *A. islandica* - oxygen isotope values– which more directly relate to temperature and hydrography if salinity variations are absent, as in SPM.

- An analysis of spatially averaged CTD (conductivity, temperature, and depth) casts on grid boxes of reduced surface area corresponding to the sectors presumed to be affected by the 18NTC. This approach is not feasible in SPM due to the paucity of available measurements, but could be attempted on the Scotian Shelf, which has been the subject of much more work over the past several decades.

- 3D numerical modeling, provided by a model that has already proven its ability to accurately reproduce diurnal tides and associated coastal trapped waves. Short simulations for different phases of the diurnal nodal cycle and for different summer stratifications can help quantify the modulation of diurnal mixing.

- Examination of other environmental archives using sclerochronology in the target areas is a natural extension of this study. Although this approach cannot provide an explanation of the chain of interactions leading to the 18NTC footprint, it may validate (or invalidate) the relatively regional nature of the influence of 18NTC on the benthic ecosystem that we describe here.

Acknowledgments

We thank the “Direction des Territoires de l’Alimentation et de la Mer (DTAM)” divers' crew (Yoann Busnot, Luc Thillais, and Jean-Marc Derouet) for their help during *A. islandica* sampling off Miquelon Island. We also thank the LEMAR (UMR 6539) Secretariat team (Anne-Sophie Podeur, Geneviève Cohat, and Yves Larsonneur) for their invaluable assistance during the administrative preparation of the field trip associated with this publication. We are sincerely grateful to the crew of the R/V Antea during the "SPM2017" survey, to the Club Nautique Saint-Pierrais for renting their boat and especially to its president, Stephane Salvat, for his incredible availability and kindness. In addition, we express our sincere gratitude to Herlé Goraguer, IFREMER delegate in SPM, for his help with local authorisations and logistics. We thank Valentin Siebert for his technical assistance during sclerochronological sample preparation. We also thank Claude Nozère, Dr. Pauline Chauvet and Dr Julien Thébault for their advice on this manuscript. We thank two anonymous reviewers and the managing editor, Prof. Alberto Piola, for significant and helpful comments which improved the manuscript quality.

Fundings

This work was supported by the EC2CO program MATISSE of the CNRS INSU, the Cluster of Excellence LabexMER, and the LIA BeBEST CNRS INEE. This research was carried out as part of the Ph.D. thesis of PP at the University of Western Brittany with a French Ministry of Higher Education and Research grant.

APPENDIX

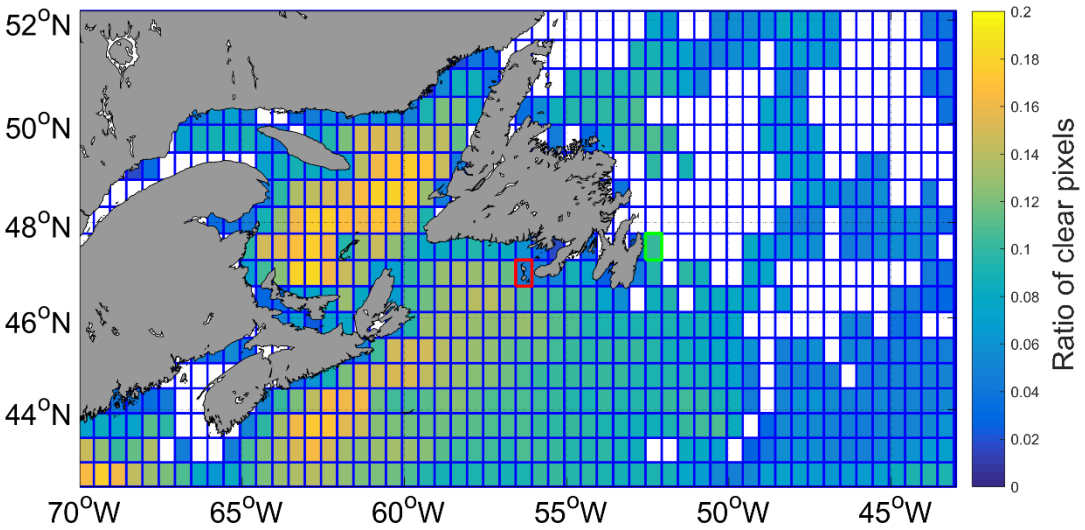

Fig. A1. Map displaying average ratio (theoretical maximum=1) of clear pixels (quality >=5) used in each grid box (33' latitude and 30' longitude including 13x12=156 pixels) for Fig. 8 August satellite SST spatial analysis (Pathfinder V5.3 dataset from Saha et al. (2018)). White boxes included at least one missing year over the 37-year time series. The green-sided rectangle circles the box used to extract August satellite SST time series from around station 27 (Fig. A2). The red-sided rectangle circles the box used to extract August satellite SST time series from Saint-Pierre and Miquelon coastal water used in Fig. 6 and 7 analyses. Due to a stroboscopic effect, 4 boxes lines contain 14x12=168 pixels. The entire domain spans 60x23 boxes.

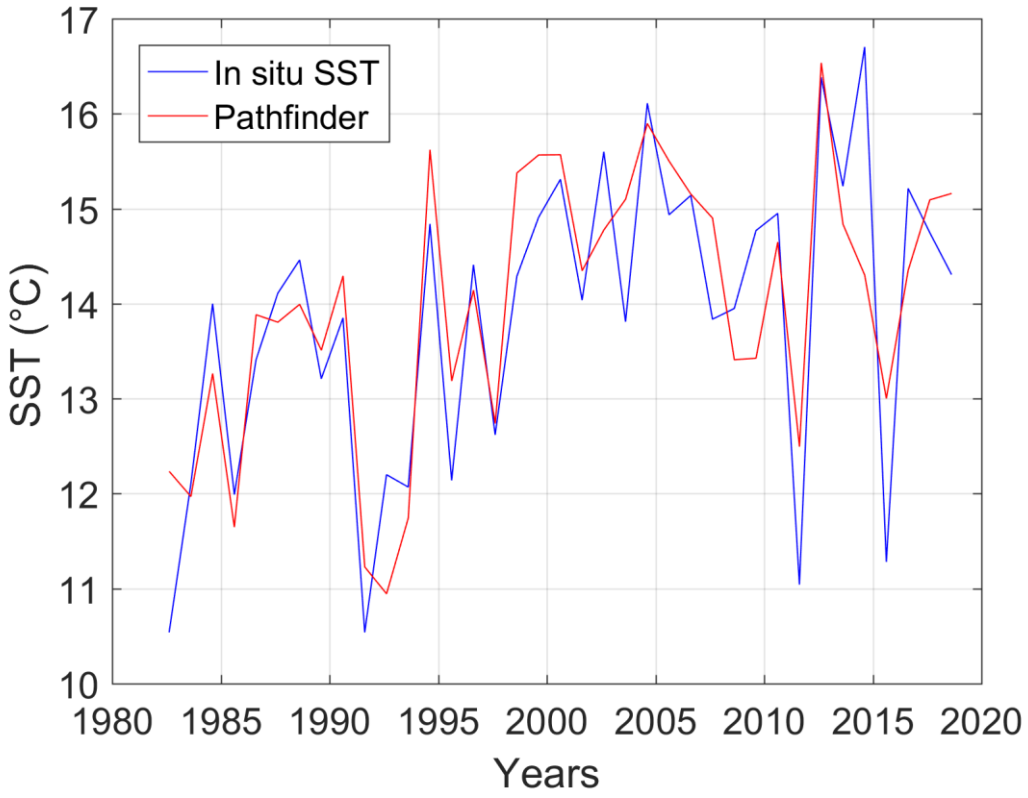

Fig. A2. Comparison of *in situ* sea surface temperatures (SST) at Station 27 and spatially averaged satellite SST from the August Pathfinder V5.3 dataset (green circled box in Fig. A1). At Station 27 (47° 33'N, 52° 35'W), monthly temperatures from surface to bottom (175 m) have been measured since the late 1940s.

References

Agosta, E.A., 2014. The 18.6-year nodal tidal cycle and the bi-decadal precipitation oscillation over the plains to the east of subtropical Andes, South America. Int. J. Climatol. 34, 1606–1614. https://doi.org/10.1002/joc.3787

Ballesta-Artero, I., Witbaard, R., Carroll, M.L., Meer, J., 2017. Environmental factors regulating gaping activity of the bivalve *Arctica islandica* in Northern Norway. Mar. Biol. 164, 116. https://doi.org/10.1007/s00227-017-3144-7.

Bezaud, M., Lazure, P., Le Cann, B., 2020. Wind-induced barotropic oscillations around the Saint Pierre and Miquelon archipelago (North-West Atlantic). Cont. Shelf Res. 195, 104062. https://doi.org/10.1016/j.csr.2020.104062

Biondi, F., Qeadan, F., 2008. Inequality in paleorecords. Ecology 89, 1056–1067. https://doi.org/10.1890/07-0783.1.

Black, B.A., Boehlert, G.W., Yoklavich, M.M., 2005. Using tree-ring crossdating techniques to validate annual growth increments in long-lived fishes. Can. J. Fish. Aquat. Sci. 62, 2277–2284. https://doi.org/10.1139/f05-142

Bunn, A.G., 2008. A dendrochronology program library in R (dplR). Dendrochronologia 26, 115–124. https://doi.org/10.1016/j.dendro.2008.01.002.

Burg, J.P., 1967. Maximum entropy spectral analysis: Presented at the 37th Annual International SEC Meeting, November I. in Oklahoma City.

Butler, P.G., Richardson, C.A., Scourse, J.D., Witbaard, R., Schöne, B.R., Fraser, N.M., Wanamaker, A.D., Bryant, C.L., Harris, I., Robertson, I., 2009. Accurate increment identification and the spatial extent of the common signal in five *Arctica islandica* chronologies from the Fladen Ground, northern North Sea. Paleoceanography 24, 2210. https://doi.org/10.1029/2008PA001715

Butler, P.G., Richardson, C.A., Scourse, J.D., Wanamaker, A.D., Shammon, T.M., Bennell, J.D., 2010. Marine climate in the Irish Sea: analysis of a 489-year marine master chronology derived from growth increments in the shell of the clam *Arctica islandica*. Quat. Sci. Rev. 29, 1614–1632. https://doi.org/10.1016/j.quascirev.2009.07.010

Butler, P.G., Wanamaker, A.D., Scourse, J.D., Richardson, C.A., Reynolds, D.J., 2013. Variability of marine climate on the North Icelandic Shelf in a 1357-year proxy archive based on growth increments in the bivalve *Arctica islandica.* Palaeogeogr. Palaeoclimatol. Palaeoecol. 373, pp. 141-151, https://doi.org/10.1016/j.palaeo.2012.01.016

Carton, J.A., Chepurin, G.A., Chen, L., 2018. SODA3: A New Ocean Climate Reanalysis. J. Clim. 31, 6967–6983. https://doi.org/10.1175/JCLI-D-18-0149.1

Chen, Z., Kwon, Y.-O., Chen, K., Fratantoni, P., Gawarkiewicz, G., Joyce, T.M., Miller, T.J., Nye, J.A., Saba, V.S., Stock, B.C., 2021. Seasonal Prediction of Bottom Temperature on the Northeast US Continental Shelf. J. Geophys. Res.-Oceans 126, e2021JC017187. https://doi.org/10.1029/2021JC017187

Cherniawsky, J.Y., Foreman, M.G.G., Kang, S.K., Scharroo, R., Eert, A.J., 2010. 18.6-year lunar nodal tides from altimeter data. Cont. Shelf Res. 30, 575–587. https://doi.org/10.1016/j.csr.2009.10.002

David, P., Delay, B., Berthou, P., Jarne, P., 1995. Alternative models for allozyme-associated heterosis in the marine bivalve *Spisula ovalis*. Genetics 139, 1719–1726.

Doré, J., Chaillou, G., Poitevin, P., Lazure, P., Poirier, A., Chauvaud, L., Archambault, P., Thébault, J., 2020. Assessment of Ba/Ca in *Arctica islandica* shells as a proxy for phytoplankton dynamics in the Northwestern Atlantic Ocean. Estuar. Coast. Shelf Sci. 237, 106628. https://doi.org/10.1016/j.ecss.2020.106628.

Douglas, A.E., 1920. Evidence of climatic effects in the annual rings of trees. Ecology 1, 24–27.

Drinkwater, K., Colbourne, E., Loeng, H., Sundby, S., Kristiansen, T., 2013. Comparison of the atmospheric forcing and oceanographic responses between the Labrador Sea and the

Norwegian and Barents seas. Prog. Oceanogr., 114, 11–25. https://doi.org/10.1016/j.pocean.2013.03.007
Flandrin, P., Rilling, G., Goncalves, P., 2004. Empirical mode decomposition as a filter bank. IEEE Signal Process. Lett. 11, 112–114. https://doi.org/10.1109/LSP.2003.821662
Garrett, C.J.R., Keeley, J.R., Greenberg, D.A., 1978. Tidal mixing versus thermal stratification in the Bay of Fundy and gulf of Maine. Atmos.-Ocean 16, 403–423. https://doi.org/10.1080/07055900.1978.9649046
Ghil, M., Allen, M.R., Dettinger, M.D., Ide, K., Kondrashov, D., Mann, M.E., Robertson, A.W., Saunders, A., Tian, Y., Varadi, F., Yiou, P., 2002. Advanced spectral methods for climatic time series. Rev. Geophys. 40, 1003. https://doi.org/10.1029/2000RG000092
Godin, G., 1972. The Analysis of Tides. University of Toronto Press, Toronto, Ont.
Good, S.A., Martin, M.J., Rayner, N.A., 2013. EN4: Quality controlled ocean temperature and salinity profiles and monthly objective analyses with uncertainty estimates. J. Geophys. Res.-Oceans 118, 6704–6716. https://doi.org/10.1002/2013JC009067
Greenan, B.J.W., Petrie, B.D., Cardoso, D.A., 2014. Mean circulation and high-frequency flow amplification in the Sable Gully. Deep-Sea Res. Part II-Top. Stud. Oceanogr. 104, 20–34. https://doi.org/10.1016/j.dsr2.2013.07.011
Grissino-Mayer, H.D., 2001. Evaluating crossdating accuracy: a manual and tutorial for the computer program COFECHA. Tree-Ring Res. 57, 205–221.
Guida, V.G., Valentine, P.C., Gallea, L.B., 2013. Semidiurnal Temperature Changes Caused by Tidal Front Movements in the Warm Season in Seabed Habitats on the Georges Bank Northern Margin and Their Ecological Implications. Plos One 8, (2):e55273. https://doi.org/10.1371/journal.pone.0055273
Halfar, J., Hetzinger, S., Adey, W., Zack, T., Gamboa, G., Kunz, B., Williams, B., Jacob, D.E., 2011. Coralline algal growth-increment widths archive North Atlantic climate variability. Paleogeogr. Paleoclimatol. Paleoecol. 302, 71–80. https://doi.org/10.1016/j.palaeo.2010.04.009
Han, G., Loder, J., 2003. Three-dimensional seasonal-mean circulation and hydrography on the eastern Scotian Shelf. J. Geophys. Res.-Oceans 108. https://doi.org/10.1029/2002JC001463
Helama, S., Schöne, B.R., Kirchhefer, A.J., Nielsen, K., Rodland, D.L., Janssen, R., 2007. Compound response of marine and terrestrial ecosystems to varying climate: pre-anthropogenic perspective from bivalve shell growth increments and tree-rings. Mar. Environ. Res. 63, 185–199. https://doi.org/10.1016/jmarenvres.2006.08.003.
Huang, N.E., Shen, Z., Long, S.R., Wu, M.L.C., Shih, H.H., Zheng, Q.N., Yen, N.C., Tung, C.C., Liu, H.H., 1998. The empirical mode decomposition and the Hilbert spectrum for nonlinear and non-stationary time series analysis. Proc. R. Soc. A-Math. Phys. Eng. Sci. 454, 903–995. https://doi.org/10.1098/rspa.1998.0193
Huthnance, J., 1978. Coastal trapped waves - analysis and numerical-calculation by inverse iteration. J. Phys. Oceanogr. 8, 74–92. https://doi.org/10.1175/1520-0485(1978)008<0074:OCTWAA>2.0.CO;2
Lazure, P., Le Cann, B., Bezaud, M., 2018. Large diurnal bottom temperature oscillations around the Saint Pierre and Miquelon archipelago. Sci. Rep. 8, 13882. https://doi.org/10.1038/s41598-018-31857-w
Lellouche, J.-M., Greiner, E., Le Galloudec, O., Garric, G., Regnier, C., Drevillon, M., Benkiran, M., Testut, C.-E., Bourdalle-Badie, R., Gasparin, F., Hernandez, O., Levier, B., Drillet, Y., Remy, E., Le Traon, P.-Y., 2018. Recent updates to the Copernicus Marine Service global ocean monitoring and forecasting real-time 1⁄12° high-resolution system. Ocean Sci. 14, 1093–1126. https://doi.org/10.5194/os-14-1093-2018
Loder, J.W., Garrett, C., 1978. The 18.6-year cycle of sea surface temperature in shallow seas due to variations in tidal mixing. J. Geophys. Res 83, 1967–1970. https://doi.org/10.1029/JC083iC04p01967.

Lyard, F., Lefevre, F., Letellier, T., Francis, O., 2006. Modelling the global ocean tides: modern insights from FES2004. Ocean Dyn. 56, 394–415. https://doi.org/10.1007/s10236-006-0086-x

Marali, S., Schöne, B.R., 2015. Oceanographic control on shell growth of *Arctica islandica* (Bivalvia) in surface waters of Northeast Iceland implications for paleoclimate reconstructions. Palaeogeogr. Palaeoclimatol. Palaeoecol 420, 138–149. https://doi.org/10.1016/j.palaeo.2014.12.016.

Marchitto, T.M., Jones, G.A., Goodfriend, G.A., Weidman, C.R., 2000. Precise temporal correlation of Holocene mollusk shells using sclerochronology. Quat. Res. 53, 236–246. https://doi.org/10.1006/qres.1999.2107.

McKinnell, S.M., Crawford, W.R., 2007. The 18.6-year lunar nodal cycle and surface temperature variability in the northeast Pacific. J. Geophys. Res.-Oceans 112, C02002. https://doi.org/10.1029/2006JC003671

McSweeney, J.M., Chant, R.J., Wilkin, J.L., 2017. Suspended-Sediment Impacts on Light-Limited Productivity in the Delaware Estuary. Estuar. Coast 40, 977–993. https://doi.org/10.1007/s12237-016-0200-3

Mette, M.J., Wanamaker, A.D., Carroll, M.L., Ambrose, W.G., Retelle, M.J., 2016. Linking large-scale climate variability with *Arctica islandica* shell growth and geochemistry in northern Norway. Limnol. Oceanogr. 61, 748–764. https://doi.org/10.1002/lno.10252

Nigam, S., Ruiz-Barradas, A., Chafik, L., 2018. Gulf Stream Excursions and Sectional Detachments Generate the Decadal Pulses in the Atlantic Multidecadal Oscillation. J. Clim. 31, 2853–2870. https://doi.org/10.1175/JCLI-D-17-0010.1

Ohashi, K., Sheng, J., Thompson, K.R., Hannah, C.G., Ritchie, H., 2009. Effect of stratification on tidal circulation over the Scotian Shelf and Gulf of St. Lawrence: a numerical study using a three-dimensional shelf circulation model. Ocean Dyn. 59, 809–825. https://doi.org/10.1007/s10236-009-0212-7

Osafune, S., Yasuda, I., 2010. Bidecadal variability in the Bering Sea and the relation with 18.6 year period nodal tidal cycle. J. Geophys. Res.-Oceans 115, C02014. https://doi.org/10.1029/2008JC005110

Osafune, S., Yasuda, I., 2006. Bidecadal variability in the intermediate waters of the northwestern subarctic Pacific and the Okhotsk Sea in relation to 18.6-year period nodal tidal cycle. J. Geophys. Res.-Oceans 111, C05007. https://doi.org/10.1029/2005JC003277

Padmanabhan, G., Rao, A.R., 1988. Maximum entropy spectral analysis of hydrologic data. Water Resour. Res. 24, 1519–1533. https://doi.org/10.1029/WR024i009p01519

Peharda, M., Schöne, B.R., Black, B.A., Corrège, T., 2021. Advances of sclerochronology research in the last decade. Paleogeogr. Paleoclimatol. Paleoecol. 570, 110371. https://doi.org/10.1016/j.palaeo.2021.110371

Peng, D., Hill, E.M., Meltzner, A.J., Switzer, A.D., 2019. Tide Gauge Records Show That the 18.61-Year Nodal Tidal Cycle Can Change High Water Levels by up to 30cm. J. Geophys. Res.-Oceans 124, 736–749. https://doi.org/10.1029/2018JC014695

Poitevin, P., Chauvaud, L., Pecheyran, C., Lazure, P., Jolivet, A., Thebault, J., 2020. Does trace element composition of bivalve shells record utra-high frequency environmental variations? Mar. Environ. Res. 158, 104943. https://doi.org/10.1016/j.marenvres.2020.104943

Poitevin, P., Thébault, J., Siebert, V., Donnet, S., Archambault, P., Doré, J., Chauvaud, L., Lazure, P., 2019. Growth Response of *Arctica Islandica* to North Atlantic Oceanographic Conditions Since 1850. Front. Mar. Sci 6. https://doi.org/10.3389/fmars.2019.00483.

Ray, R.D., 2007. Decadal climate variability: Is there a tidal connection? J. Clim. 20, 3542–3560. https://doi.org/10.1175/JCLI4193.1

Reynolds, R.W., Smith, T.M., Liu, C., Chelton, D.B., Casey, K.S., Schlax, M.G., 2007. Daily High-Resolution-Blended Analyses for Sea Surface Temperature. J. Clim. 20, 5473–5496. https://doi.org/10.1175/2007JCLI1824.1

Robin, N., 2007. Morphodynamique des systèmes de flèches sableuses : Étude entre les embouchures tidales de l'Archipel de St Pierre et Miquelon et de la côte ouest du Cotentin (Manche ([PhD dissertation].). Université de Caen / Basse Normandie, Caen (Fr).

Saha, K., Zhao, X., Zhang, H.-M., Casey, K.S., Zhang, D., Baker-Yeboah, S., Kilpatrick, K.A., Evans, R.H., Ryan, T., Relph, J.M., 2018. AVHRR Pathfinder version 5.3 level 3 collated (L3C) global 4km sea surface temperature for 1981-Present. [August 1982-August 2018]. NOAA National Centers for Environmental Information. Dataset. https://doi.org/10.7289/v52j68xx.

Schöne, B.R., Houk, S.D., Freyre Castro, A.D., Fiebig, J., Kröncke, I., Dreyer, W., Oschmann, W. 2005. Daily growth rates in shells of *Arctica islandica*: assessing subseasonal environmental controls on a long-lived bivalve mollusk. Palaios 20, 78–92. https://doi.org/10.2110/palo.2003.p03-101

Schöne, B.R., 2013. *Arctica islandica* (Bivalvia): a unique paleoenvironmental archive of the northern North Atlantic Ocean. Glob. Planet. Change 111, 199–225. https://doi.org/10.1016/j.gloplacha.2013.09.013.

Sharples, J., 2008. Potential impacts of the spring-neap tidal cycle on shelf sea primary production. J. Plankton Res. 30, 183–197. https://doi.org/10.1093/plankt/fbm088

Simpson, J., Hunter, J., 1974. Fronts in Irish Sea. Nature 250, 404–406. https://doi.org/10.1038/250404a0

Thomson, D., 1982. Spectrum Estimation and Harmonic-Analysis. Proc. IEEE 70, 1055–1096. https://doi.org/10.1109/PROC.1982.12433

Vautard, R., Ghil, M., 1989. Singular Spectrum Analysis in Nonlinear Dynamics, with Applications to Paleoclimatic Time-Series. Physica D 35, 395–424. https://doi.org/10.1016/0167-2789(89)90077-8

Vianna, M.L., Menezes, V.V., 2013. Bidecadal sea level modes in the North and South Atlantic Oceans. Geophys. Res. Lett. 40, 5926–5931. https://doi.org/10.1002/2013GL058162

Wang, Y., Sheng, J., Lu, Y., 2020. Examining tidal impacts on seasonal circulation and hydrography variability over the eastern Canadian shelf using a coupled circulation-ice regional model. Prog. Oceanogr. 189, 102448. https://doi.org/10.1016/j.pocean.2020.102448

Wigley, T.M.L., Briffa, K.R., Jones, P.D., 1984. On the average value of correlated time series, with applications in dendroclimatology and hydrometeorology. J. Appl. Meteorol. Clim 23, 201–213. https://doi.org/10.1175/1520-04501984023

Witbaard, R., Duineveld, G.C.A., Bergman, M. 2001. The effect of tidal resuspension on benthic food quality in the southern North Sea. Senckenberg. Marit., 31 (2001), pp. 225-234. https://doi.org/10.1007/BF03043031

Wolfe, C.L.P., Hameed, S., Chi, L., 2019. On the Drivers of Decadal Variability of the Gulf Stream North Wall. J. Clim. 32, 1235–1249. https://doi.org/10.1175/JCLI-D-18-0212.1

Xu, Z., Loder, J., 2004. Data assimilation and horizontal structure of the barotropic diurnal tides on the Newfoundland and southern Labrador Shelves. Atmos.-Ocean 42, 43–60. https://doi.org/10.3137/ao.420104

Zhao, C., Daewel, U., Schrum, C., 2019. Tidal impacts on primary production in the North Sea. Earth Syst. Dynam. 10, 287–317. https://doi.org/10.5194/esd-10-287-2019